



## Practical considerations for small receive coils in surface NMR

Denys Grombacher<sup>a,\*</sup>, Lichao Liu<sup>a</sup>, Jakob Juul Larsen<sup>b</sup>, Esben Auken<sup>a</sup>

<sup>a</sup> Geoscience Department, Aarhus University, Aarhus, Denmark

<sup>b</sup> Department of Engineering, Aarhus University, Aarhus, Denmark

### ARTICLE INFO

#### Article history:

Received 10 September 2017

Received in revised form 5 March 2018

Accepted 8 April 2018

Available online 09 April 2018

### ABSTRACT

The development of multichannel instrumentation was a significant step forward for surface nuclear magnetic resonance (NMR). Multichannel instruments allow data to be recorded on multiple receivers simultaneously, thus facilitating the exploitation of Wiener filtering techniques that provide significant signal-to-noise increases and allow two- and three-dimensional images of the subsurface properties to be produced. When working in challenging environments (e.g. forested/brushy terrain), difficult noise conditions, or when using complicated survey designs it can become quite cumbersome to deploy multiple coils, which often require substantial lengths of cable to be deployed. As such, it would be advantageous if the dimensions of typical receive coils could be greatly reduced from the current standards (~25–100 m). The use of small receive coils would lead to more rapid survey deployment and may advance the utility of methods requiring multiple receivers. The objectives of this work are two-fold. The first aims to quantify limits on the feasible dimensions of small receive coils in surface NMR, aiming to provide an estimate of the minimum effective area of a functional surface NMR receiver. The second aims to demonstrate that the use of multiple additional small receive coils (when used in conjunction with the standard large coincident transmit/receive coil) can help to improve the resolution of estimated water content and relaxation time depth profiles. Synthetic results are presented to quantify lower effective area limits and to demonstrate potential resolution improvements provided by small receivers. The feasibility of a small receiver (400 m<sup>2</sup> and 200 m<sup>2</sup>) is demonstrated in a field setting.

© 2017 Elsevier B.V. All rights reserved.

### 1. Introduction

The surface nuclear magnetic resonance (NMR) method involves the use of surface coils to investigate aquifer properties at depth. Traditionally, a single coil serves as both the transmit and receive coil (Legchenko and Valla, 2002). In the single coil configuration, referred to as a coincident loop set up, the surface NMR measurement is generally used to produce depth profiles of the water content and relaxation times. The shape of the single coil is often a square loop, circular loop, or a figure-eight loop (Trushkin et al., 1994) with dimensions (side length/diameter) of ~25 m to 100 m. Larger loop sizes help to increase depth penetration and improve resolution at the greatest depths (Müller-Petke and Yaramanci, 2008).

Following the development of multi-channel surface NMR instruments (Radic, 2006; Walsh, 2008), which facilitate the ability to measure signals on independent coils simultaneously, it has become common to deploy multiple coils during a surface NMR measurement. The decision to use multiple coils is often based upon two factors. The first is a desire to exploit Wiener filtering advancements (Walsh, 2008; Dalggaard et al., 2012; Müller-Petke and Costabel, 2014) that

have helped to greatly improve the signal-to-noise ratio (SNR) of surface NMR measurements. Wiener filtering requires the deployment of a secondary coil called a reference coil, that functions to collect noise-only data, which is accomplished by placing the coil a large distance away from the transmit coil. If the characteristics of the noise measured in the reference loop are correlated with that in the main receive loop Wiener filtering can be used to improve SNR. A second reason to deploy multiple coils is to produce two- or three-dimensional images of subsurface water content and relaxation times (Hertrich et al., 2005; Hertrich et al., 2007; Legchenko et al., 2011). For two- or three-dimensional measurements one coil functions as the transmitter, while all coils function as receivers. In subsequent measurements each coil is used as the transmitter and the coils may be moved in a “roll-along” fashion to cover large transects or areas (Hertrich et al., 2009). Jiang et al. (2015) demonstrated an alternative approach to produce two-dimensional images that does not require a “roll-along” approach instead proposing the use of a single elongated transmit coil with several smaller receive coils placed within thus allowing the full transect to be measured following each transmit pulse. This approach has the potential to greatly improve measurement speeds of two- and three-dimensional surface NMR surveys. Behroozmand et al. (2016) also propose to use a separate receive coil in the context of a one-dimensional depth profile, where a central-loop configuration involving a smaller

\* Corresponding author.

E-mail address: [denys.grombacher@geo.au.dk](mailto:denys.grombacher@geo.au.dk). (D. Grombacher).

receive loop placed in the center of a larger transmit loop is shown to enhance SNR and improve resolution. In each of these cases, the typical coil dimensions are ~25–100 m (side length/diameter). The potential of a multi-axis surface NMR receiver, which by necessity must be small, has also been recently explored (Kass et al., 2017).

In practice, deployment of many coils can quickly become quite cumbersome and may require that vast lengths of cable are laid out, which can become challenging in difficult environments such as forests or brushy terrain. To improve the utility of techniques requiring multiple coils, there is a growing desire to employ coils much smaller than those traditionally employed in surface NMR. Small coils would be greatly advantageous for mobile/rapid collection surface NMR systems (Grunewald and Walsh, 2016). Davis et al. (2014) employed a SQUID magnetometer as a surface NMR receiver, demonstrating the potential for a dipole-like receiver in surface NMR. Small receive coils (~1–6 m in dimension) have also been investigated for applications in underground magnetic resonance sounding (MRS) for water quantification in tunnels (Greiben et al., 2011; Lin et al., 2017) due to geometry constraints imposed by the tunnel dimensions.

The objectives of this study are two-fold: 1) we aim to quantify potential limits on the feasible dimensions of small surface NMR receive coils (where we consider the case of a traditional air-core induction coil) and 2) we aim to demonstrate potential resolution benefits for a survey design employing several small receive coils in addition to the standard large coincident receiver. The use of complementary small receive coils (that measure the NMR signal) is motivated by a desire to adapt approaches employed in magnetic resonance imaging (MRI) to the surface NMR setting, where the use of small secondary receive coils have been demonstrated in MRI to improve measurement speed (Carlson and Minemura, 1993; Pruessmann et al., 1999) and resolution (Pruessmann et al., 2001; Weiger et al., 2002). We focus on the scenario where small receive coils are used in conjunction with a larger transmit coil. Recommendations for the design of untuned small coils for use in both reference noise cancellation approaches and to receive surface NMR signals are given. Numerical simulations are presented to demonstrate favorable survey designs capable of improving the performance of small surface NMR receivers. The use of small receive coils that measure the surface NMR signal embedded within a larger transmitter (in addition to the large coincident receiver) is also shown to improve the resolution of surface NMR depth profiles. Field results are also presented to validate the feasibility of small surface NMR receive coils.

## 2. Background

The primary requirement of a functional surface NMR receiver is that it provide an adequate SNR. This demands that the receive coil is capable of measuring a satisfactory amplitude NMR signal while mitigating noise to an acceptable level. Consider first several factors affecting the measured noise levels. For the purposes of this discussion we group noise sources into two categories: 1) noise that originates from the receive electronics/cable (internal noise  $n_{int}$ ), and 2) noise that originates from external sources (i.e. noise that either inductively or capacitively couples to the receive coil). Category 1 is dominated by Johnson (thermal) noise that originates from the coil resistance and the input noise of the preamplifier. Johnson noise is described by

$$n_j = \sqrt{4k_b T \frac{\rho L}{A}} \quad (1)$$

$n_j$  is given in units of  $V/Hz^{1/2}$ .  $T$  is the temperature of the wire,  $\rho$  is the wire resistivity,  $L$  is the wire length, and  $A$  is the cross-sectional area of the wire. If we consider representative values of  $T = 293$  K,  $\rho = 1.72e-8$   $\Omega m$  (resistivity of copper), and  $A = 8.24e-7$   $m^2$  (cross-sectional area of a 18 gauge wire with a 1.024 mm diameter), then  $n_j \sim (L)^{1/2} \cdot 18$   $pV/Hz^{1/2}$ .  $L$  is the total length of wire in the receive coil. Note that Eq. (1) corresponds to the case of an untuned coil, where the coil gain

factor is 1 over the frequency range of interest. We consider only the untuned receive coil scenario. The input noise of the preamplifier is the most critical factor determining the noise level of the receive electronics (not including Johnson noise). Fig. 1 illustrates a schematic showing the signal chain of the surface NMR receiver.

Signals measured by the receive coil are initially amplified using a pre-amplifier (with a gain of 21 for the receiver used in this study) before being further amplified (by additional amplifiers), filtered (e.g. using a band-pass (BP) filter), and recorded by the analog to digital converter (ADC). Because the preamplifier has a gain of 21, its internal noise level is amplified to a much higher level than the noise created by components further down the signal chain. Therefore, it is the input noise of the preamplifier that is most critical. The input noise of the receiver is determined by shorting the input of the preamplifier and measuring the voltage recorded by the receiver (i.e. the signal digitized by the ADC in Fig. 1). The corresponding noise level contains contributions from all components in the signal chain in Fig. 1 except the coil. This effectively represents the lowest possible effective noise level and is set by the components/design of the receiver board (but is effectively dominated by the preamplifier). For the receive system used in this manuscript, the Apsu receiver developed at Aarhus University (Liu et al., 2017), the input noise ( $n_{in}$ ) of the preamplifier is 1.78  $nV/Hz^{1/2}$  (based upon a single one second recording). Note that the Apsu receiver is a differential receive system, which leads to a slightly higher input noise level because two signals that are amplified by two separate preamplifiers are combined. For an unbalanced receiver where only a single preamplifier is employed the input noise could be reduced to ~1.2  $nV/Hz^{1/2}$  (if we consider a single preamplifier for the Apsu receiver) at the expense of increased common mode noise. Comparing  $n_j$  and  $n_{in}$  indicates that wire lengths of several kilometers are required for these two noise sources to produce similar levels of noise (for the considered 1.024 mm diameter wire). Note that preamplifier improvements (or alternative preamplifier designs) that may reduce the input noise could lead to scenarios where  $n_j$  is no longer much less than  $n_{in}$ . Larger diameter wire could be used to further reduce the magnitude of Johnson noise. In the following we consider the internal noise level to be effectively determined by the input noise as the coils we intend to employ do not exceed lengths of several kms. Therefore, the input noise and filter bandwidths set a threshold, where a functioning receiver must be able to measure a signal that exceeds this threshold. If the Johnson noise is not negligible compared to the input noise the threshold should take both noise sources into account. To convert the internal noise into an estimated root mean square (RMS) noise amplitude in the time domain ( $n_{RMS, in}(t)$ )  $n_{in}$  is multiplied by the square root of the filter bandwidths (BW), typically the bandwidth of the digital bandpass filters used during data processing,

$$n_{RMS, in}(t) = n_{in} \sqrt{BW} \quad (2)$$

At this point it is convenient to consider two scenarios based upon the desired function of the receiver; that is, we will consider the case where a receiver functions as a reference loop (that measures noise only) separately from the case where a receiver intends to measure the NMR signal. The reason for considering these two scenarios separately is that the NMR signal detection case involves additional factors. Consider first the scenario where the receiver is to be used as a reference loop. In this case, the “signal” we aim to measure is the noise that

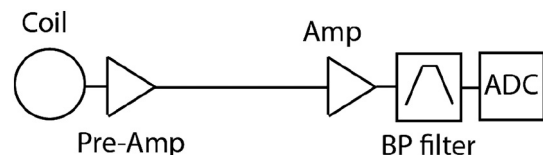


Fig. 1. Signal chain for the surface NMR receiver employed in this study.

originates from external sources (referred to as  $n_{ext}$ ). External noise sources include powerline harmonics (Legchenko and Valla, 2003; Larsen et al., 2014), sferics, electric fence spikes (Plata and Rubio, 2002; Legchenko, 2007; Jiang et al., 2011; Dalgaard et al., 2014; Costabel and Müller-Petke, 2014; Larsen, 2016), and other anthropogenic/ambient noise sources. As a result, a functional receiver deployed as a reference loop must be capable of ensuring that  $n_{ext}$  exceeds  $n_{in}$ . A simplified description of  $n_{ext}$  is given by

$$n_{ext} = n_{ext/m^2} A_{eff}. \quad (3)$$

$n_{ext/m^2}$  (units of  $V/Hz^{1/2}/m^2$ ) represents an approximation of the square root of the power spectral density (PSD) of the external noise across the bandwidth of interest that would be measured by a coil with an effective area of  $1 m^2$ . In practice this value is measured by recording a noise-only time series and calculating the resulting PSD. In surface NMR the frequency band of interest ranges from  $\sim 1$ – $3$  kHz (depending on the local magnitude of Earth's field).  $A_{eff}$  is the effective area of the receive coil and scales  $n_{ext/m^2}$ . To determine the minimum acceptable coil area  $n_{ext/m^2}$  must be measured and an appropriate  $A_{eff}$  determined to ensure that  $n_{ext}$  exceeds  $n_{in}$ . If this condition is not satisfied the utility of the receiver to function as a reference coil will be reduced because much of the measured noise will not originate from external noise sources that also impact the main signal loop thus reducing the correlation of the noise measured in the signal and reference loops. We do not consider in the following the influence of the coil size on  $n_{ext}$ ; that is, we assume that coils of different sizes/number of turns but with equivalent  $A_{eff}$  will measure the same  $n_{ext}$ . Nyboe and Sørensen (2012) observed  $n_{ext}$  to range from  $\sim 0.02$ – $1$   $nV/Hz^{1/2}/m^2$  in the  $1$ – $3$  kHz frequency band at several sites around Denmark. Noise measurements conducted at four additional sites in the vicinity of Aarhus, Denmark demonstrated similar noise levels of  $\sim 0.01$   $nV/Hz^{1/2}/m^2$  in the  $1$ – $3$  kHz frequency. The challenge is that external noise levels can be extremely variable both temporally and spatially and values smaller and larger than these observations are possible. Comparing the observed  $n_{ext/m^2}$  with  $n_{in}$  suggests that an  $A_{eff}$  of  $\sim 200 m^2$  is likely to ensure that  $n_{ext}$  is greater than  $n_{in}$  (e.g.  $200 m^2 \times 0.01$   $nV/Hz^{1/2}/m^2 > 1.78$   $nV/Hz^{1/2}$ ). Note that the  $200 m^2$  reference coil should perform as desired at higher noise levels but will drop below the input noise level if lower external noise levels are present. Given the innate unpredictability of  $n_{ext/m^2}$  we recommend that this threshold is exceeded in practice in order to extend the range of measurable  $n_{ext/m^2}$  to even lower levels.

For scenarios where the receiver will be used to detect the NMR signal the receiver must be capable of ensuring a minimum detection threshold is achieved, which requires that the receiver is capable of measuring a signal  $S_{net}$  that at least exceeds the threshold set by the internal noise. A simplified version of the signal  $S_{net}$  is given by

$$S_{net} = \left( S_{NMR/m^2} + n_{ext/m^2} \sqrt{BW} \right) A_{eff}, \quad (4)$$

where  $S_{NMR/m^2}$  is the amplitude of the NMR signal measured per square meter of receiver area. Two factors must be considered to determine the minimum acceptable coil area for a receiver that intends to detect an NMR signal. The first is that the  $n_{ext}$  component of  $S_{net}$  must exceed  $n_{in}$ , otherwise the effectiveness Wiener filtering will be reduced. The second and most important factor, is that the receiver must be able to receive an NMR signal. This requires that the  $S_{NMR}$  component of  $S_{net}$  exceeds the noise level. In practice the NMR signal amplitude ( $S_{NMR/m^2}$ ) is affected by many factors, such as the transmit coil geometry, receive coil geometry, amplitude of the current pulse, and properties of the subsurface. A detailed derivation of the surface NMR forward problem highlighting all factors influencing the surface NMR signal is given in Weichman et al. (2000). In the following section we investigate factors such as receive coil size, receive coil location within the transmit loop,

and current amplitude. We consider two excitation schemes (an on-resonance excitation pulse and an adiabatic half passage pulse). This sensitivity analysis will be used to quantify a representative value of  $S_{NMR/m^2}$  in order to estimate the lower threshold of acceptable  $A_{eff}$ .

### 3. Results

#### 3.1. Limits on small receive coil dimensions

To quantify the lower limit of acceptable  $A_{eff}$  for a receiver intended to measure an NMR signal,  $S_{NMR/m^2}$  must be quantified. To estimate  $S_{NMR/m^2}$  the kernel matrix  $\mathbf{K}$  associated with various receive configurations is calculated using AarhusInv (Auken et al., 2014) with the implementation described in Behroozmand et al. (2012). From the kernel matrix sounding curves are formed (by integrating the kernel over all depths). Sounding curves provide a simple approach to quantify the expected initial amplitude of the surface NMR signal following each pulsed current amplitude and represent a convenient metric to determine the expected signal amplitude from a particular survey design. Note that all sounding curves shown in the following are normalized by the coil area. We consider the scenario where small receiver coils are used in conjunction with a larger transmit coil, similar to the scenarios proposed by Jiang et al. (2015) and Behroozmand et al. (2016). The transmit coil in each case is a  $100 m$  by  $100 m$  square coil, the inclination is  $70^\circ$ , the Larmor frequency is  $2049$  Hz, and 16 current amplitudes spanning from  $1.85$  to  $213.25$  A are used. The subsurface is a  $1000 \Omega m$ ,  $100\%$  water content half-space. For each receive configuration, sounding curves are produced for an excitation scheme employing a  $40$  ms on-resonance pulse and again for an adiabatic half passage pulse (described by the numerically optimized modulation (NOM) approach discussed in Grombacher (2018), where the NOM pulse recommended in that paper is used). This provides the opportunity to examine if a particular excitation scheme exhibits advantages for the small receiver scenario.

Given a fixed transmit geometry, the survey design is determined by several parameters describing the geometry of receive coil. In the following we investigate the impact of the receiver size and receiver position. Consider first the impact of receiver size on  $S_{NMR/m^2}$ . Fig. 2 illustrates the sounding curves produced by surveys employing receive coils of varying sizes (each color corresponds to a particular receiver size). Fig. 2C illustrates the receiver size; receivers side lengths of [100 75 50 25 15 10 5 1] m are investigated (profile colors correspond to the receiver size). Each receiver is centered at the center of the transmit coil. The transmit loop is the size of the red square ( $100 m$  by  $100 m$ ). Fig. 2A illustrates the absolute value of the sounding curves produced by a  $40$  ms on-resonance pulse. Fig. 2B illustrates the absolute value of the sounding curves produced by an example adiabatic pulse. Each sounding curve is normalized by the receive coil area. For the on-resonance case, the smaller receive coils produce larger signal amplitudes for intermediate currents ranging from  $\sim 10$ – $15$  A to  $\sim 100$  A, while the largest receive loop (red) produces a larger signal amplitude at currents less than  $\sim 10$ – $15$  A and greater than  $\sim 100$  A. The larger amplitude sounding curves for the smaller receive loops at intermediate currents is consistent with the observations of Behroozmand et al. (2016), where a  $100 m$  receive loop was compared against a  $25 m$  receiver (that shares the same center point). Small and large coils measure different signals per square meter of area because their receive sensitivities differ spatially. For certain current strengths, the small coil's receive sensitivity is stronger at the signal origin (leading to larger signal amplitudes) while in other cases the large coil's sensitivity is stronger at the signal origin. For the adiabatic pulse (Fig. 2B) the smallest receive coils produce larger signal amplitudes at the largest currents, while the largest receiver produces the largest signals at small currents. Overall, Fig. 2A and B indicate that small receivers may provide a more efficient use of coil area over certain current ranges. More efficient in this context means that they are able to produce a larger signal

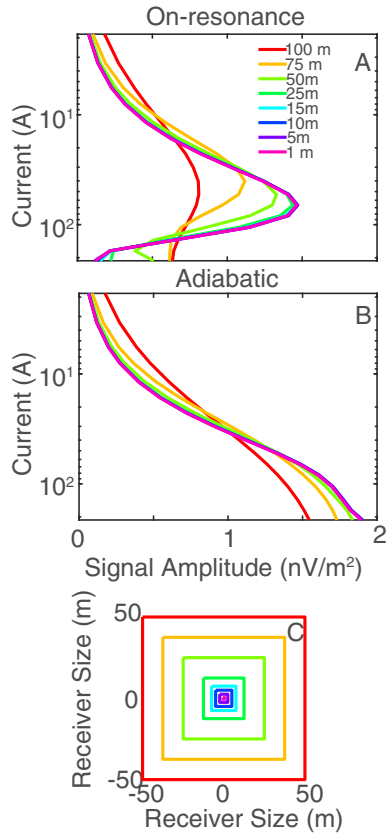


**Fig. 2.** A) and B) show area normalized sounding curves for a survey employing a 100 m by 100 m square transmitter and a separated receiver of varying size. A) and B) illustrate the sounding curves following a 40 ms on-resonance pulse and an example adiabatic pulse, respectively. Profile colors correspond to the relevant receiver size shown in C.

amplitude given the same  $A_{eff}$ . At small currents, the large receiver appears to be a more efficient use of coil area. Taken together, the ability of small or large receivers to provide more efficient use of coil area over different current ranges suggests that it may be beneficial to employ both large and small receive coils. Fig. 2 also indicates that the sounding curves show little variation for receive coils below ~10–15 m in side length. Below a certain size the receivers approach the behavior expected for a dipole receiver (with the appropriate moment) resulting in the light blue to magenta sounding curves converging towards a similar behavior. This suggests that equivalent performance can be expected from coils of different sizes but equal  $A_{eff}$  (due to different numbers of turns) as long as the side length is below ~10–15 m.

To investigate whether alternative receive coil locations impact the expected signal amplitudes, Fig. 3 illustrates the absolute value of the sounding curves produced by a 1 m by 1 m receive coils placed at varying locations within a 100 m by 100 m square transmitter. Fig. 3E and F illustrate the location of the receive coil for each scenario and the corresponding profile color (the left and right columns illustrate sounding curves for the receiver locations shown in 3E and 3F, respectively). The top and middle rows correspond to sounding curves produced by the same on-resonance and adiabatic pulse used in Fig. 2, respectively. In the left column the receive coil is located at  $x = [-30 -20 -10 0 10 20 30]$  m with  $y = 0$  m in each case, where the center of the transmit loop occurs at  $x = 0$  m and  $y = 0$  m. North points in the  $x$ -direction. Fig. 3A and C indicate that moving the receive coil towards the northern edge of the transmit coil increases the signal amplitude substantially for both the on-resonance and adiabatic pulses. For the on-resonance pulse, as the receiver approaches the southern edge of the transmit coil the real sounding curves begin to show strongly oscillatory behavior (not shown), which results in the sharper variations in the absolute

sounding curves at large currents (red curve). The source of the discrepancy between southern/northern offsets arises from an asymmetry that exists in the spatial distribution of the excited magnetization due to the inclination of Earth's field. Given an inclination of  $70^\circ$  (as in this example), the lobe of excited magnetization under the northern edge of the loop penetrates both deeper and covers a larger area. As such, moving a receiver closer to this larger excited magnetization lobe results in a larger signal amplitude. In the right column the receive coil is located at  $y = [-30 -20 -10 0 10 20 30]$  m with  $x = 0$  m in each case. In this case, the absolute sounding curves display less sensitivity to receiver location. For the on-resonance pulse a symmetry between positive and negative  $y$ -offsets is observed, while for the adiabatic case a stronger variation with  $y$ -offset (east/west offset) is observed. The reason for the breakdown in symmetry for the adiabatic case is due to the combination of phases that arise directly from the excitation pulse and those from the receiver location (geometric phase). The on-resonance symmetry (for equal magnitude east/west offsets) is also broken if the subsurface has strong conductivity (not shown). Overall, Fig. 3 demonstrates that the position of the small receiver within the transmit loop can have a strong influence on the measured signal and that a small receiver located in the northern half of the loop produces the largest signal.

In order to determine a threshold for the minimum  $A_{eff}$  we must select a representative  $S_{NMR}/m^2$  value. From the sounding curves in Figs. 2 and 3 a signal amplitude of ~0.25 nV/m<sup>2</sup> appears to be a representative value describing the lower end of the expected signal amplitudes for a range of receiver locations/current amplitudes. Although exact signal amplitudes depend on both receiver location and current amplitude, most amplitudes are observed to exceed this lower 0.25 nV/m<sup>2</sup> value. Only the smallest investigated currents dip below these signal amplitudes. However, these signal amplitudes correspond to sounding curves formed by integrating the kernel matrix  $\mathbf{K}$ , and effectively represent the signal amplitudes expected for a 100% water content subsurface. In practice the sounding curves contain an additional weighting due to the true subsurface water content distribution. To define a minimum detection threshold we consider the signal amplitude that would be measured in the presence of a 5% water content half-space. This scenario represents a low water content/low signal amplitude environment. If a minimum  $A_{eff}$  is selected to ensure that a satisfactory signal amplitude can be measured in this low water content limit, a receiver with the same  $A_{eff}$  could also be expected to perform well in more favorable circumstances. For the 5% water content half-spaces, the lower end of expected  $S_{NMR}/m^2$  for a small receiver is approximately ~0.0125 nV/m<sup>2</sup> (formed by multiplying the previous 0.25 nV/m<sup>2</sup> by 0.05). In addition to a lower  $S_{NMR}/m^2$  estimate, a reference noise level is required in order to determine a minimum  $A_{eff}$  threshold. In practice the total noise will be the combination of  $n_{ext}$  and  $n_{in}$  where the total noise  $n_{tot}$  is given by

$$n_{tot}(t) = \sqrt{(n_{ext}/m^2 A_{eff})^2 + (n_{in})^2 \sqrt{BW} / \sqrt{N_{stack}}}. \quad (5)$$

$N_{stack}$  corresponds to a minimum stack number. Determining  $n_{tot}$  is challenging due to the fact that  $n_{ext}/m^2$  is not known a priori. Furthermore,  $n_{ext}/m^2$  is extremely site dependent and temporally varying. To address uncertainty in the magnitude of  $n_{ext}/m^2$  Fig. 4A illustrates the SNR ( $SNR = S_{NMR}/m^2 A_{eff} / n_{tot}$ ) as a function of  $A_{eff}$  for three magnitudes of  $n_{ext}/m^2$  given an  $S_{NMR}/m^2 = 0.0125$  nV/m<sup>2</sup>,  $n_{in} = 1.78$  nV/Hz<sup>1/2</sup>,  $N_{stack} = 16$  and  $BW = 200$  Hz. Four values of  $n_{ext}/m^2$  equal to  $[0.01 0.1 1 10] \times 0.0125$  nV/Hz<sup>1/2</sup>/m<sup>2</sup> are investigated (light grey to black lines for increasing  $n_{ext}/m^2$ ). These  $n_{ext}/m^2$  levels correspond to RMS noise levels of ~[4 44 442 4420] nV in a 100 m by 100 m square loop for  $BW = 200$  Hz and  $N_{stack} = 16$ . Note that both smaller and larger values of  $n_{ext}/m^2$  are possible, these particular values are chosen to demonstrate a possible range of behaviors (from a very low to very high noise conditions). In practice, the low noise limit may be achieved given effective power line harmonic removal and Wiener filtering. In addition to the four  $n_{ext}/m^2$  cases, we also illustrate the best-case scenario where  $n_{ext}/m^2 = 0$

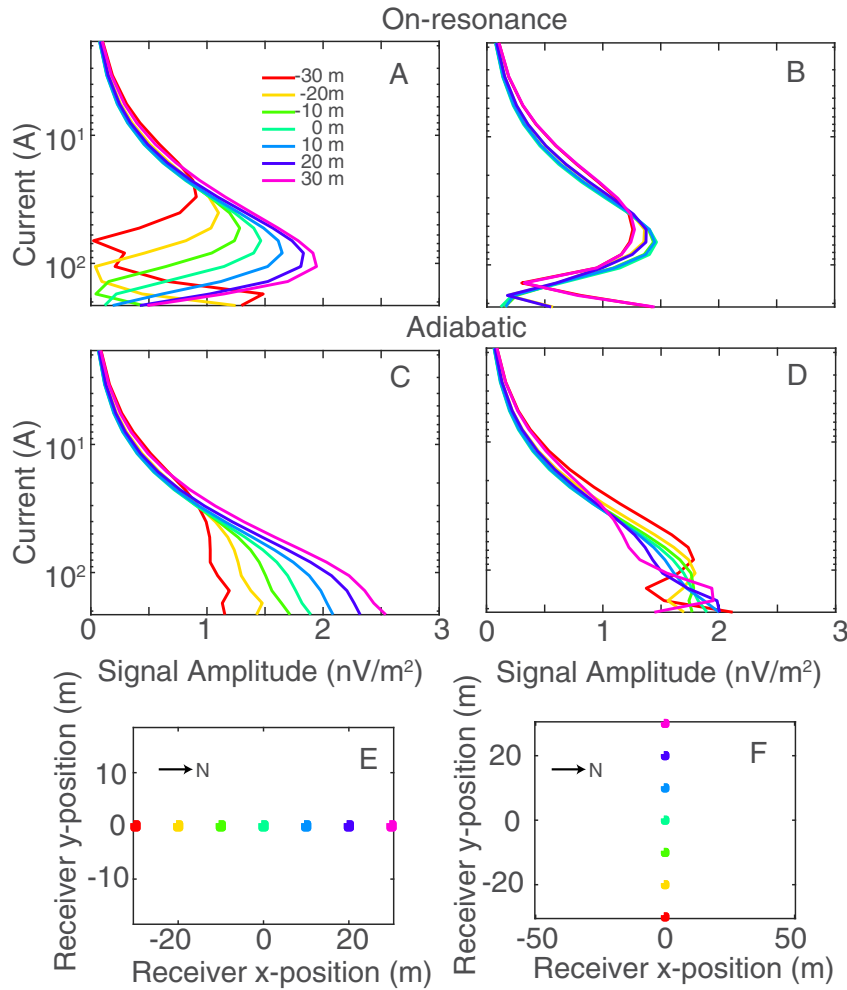


**Fig. 3.** The top and middle rows illustrate the absolute sounding curves for synthetic surveys using a 100 m by 100 m transmitter with a 1 m<sup>2</sup> receiver located at varying locations for a 40 ms on-resonance pulse and an adiabatic pulse (same as in Fig. 2), respectively. E) and F) illustrate the locations (and relevant colors) of the small receiver for the left and right columns, respectively.

(dashed-black line). Three regimes can be observed in Fig. 4A. In the first regime (light grey line), where  $n_{tot}$  is dominated by  $n_{in}$ , the SNR ( $A_{eff}$ ) curves closely track the dashed-black line. This case represents the optimal low external noise scenario where SNR can be improved by increasing  $A_{eff}$ . The second regime occurs when  $n_{tot}$  becomes dominated by  $n_{ext}$ , which manifests as the horizontal asymptotic behavior. In this limit, SNR is effectively locked and further  $A_{eff}$  increases do not produce any significant SNR improvements. The third scenario is the mixed case where the SNR( $A_{eff}$ ) curves begin to deviate from the black dashed line and approach the horizontal asymptotes, which occurs when  $n_{ext}/m^2 A_{eff} \approx n_{in}$ . In this mixed case, the SNR is less than the asymptotic value over a certain  $A_{eff}$  interval. The challenge now becomes defining an  $A_{eff}$  threshold that can balance performance in as many noise conditions as possible. In the large  $n_{ext}/m^2$  limit the SNR( $A_{eff}$ ) curves quickly asymptote and little advantage is gained from further increasing  $A_{eff}$ . In the small  $n_{ext}/m^2$  limit, the SNR is very poor (i.e.  $\ll 1$ ) at the smallest  $A_{eff}$ . To improve SNR in the small  $n_{ext}/m^2$  limit  $A_{eff}$  can be increased. Given the stated desire to work with small coils, increasing  $A_{eff}$  will likely involve increasing the number of turns which places practical limitations on the achievable  $A_{eff}$ , as increasing the number of turns could increase the coil's self-capacitance and inductance to a point where the coil's cutoff frequency approaches the frequency band of interest. Therefore, it becomes practical to define a lower  $A_{eff}$  threshold that can at least satisfy a minimum detection threshold of SNR = 1 in the low water content scenario.

We propose a pragmatic approach to define the lower  $A_{eff}$  threshold where the threshold is determined in the low  $n_{ext}/m^2$  limit. This approach has the benefit that the threshold is based upon site independent values such as the input noise and expected signal amplitudes for a low water content halfspace. From Fig. 4A the detection threshold of SNR = 1 in the low  $n_{ext}/m^2$  limit is satisfied if  $A_{eff}$  is greater than  $\sim 500$  m<sup>2</sup>. However, in practice the net SNR will also be affected by  $n_{ext}/m^2$ ; the difficulty is that  $n_{ext}/m^2$  is not known a priori and can exhibit strong temporal and spatial variation. Fig. 4B illustrates the range of  $n_{ext}/m^2$  where the  $A_{eff} = 500$  m<sup>2</sup> satisfies the SNR=1 objective. Fig. 4B shows SNR as a function of  $n_{ext}/m^2$  for a 500 m<sup>2</sup> coil (black line), a 1000 m<sup>2</sup> coil (dark grey line), and a 10,000 m<sup>2</sup> coil (light grey line) for the same signal and input noise levels considered in Fig. 4A. The 10,000 m<sup>2</sup> case is considered to represent the asymptotic SNR value for a large coil. The dashed black line highlights the SNR = 1 criteria. The black line approximates approaches the SNR = 1 line in the low  $n_{ext}/m^2$  limit as expected, while also converging towards the light grey line in the large  $n_{ext}/m^2$  limit. This indicates that if a coil has an area equal to or exceeding the 500 m<sup>2</sup> threshold it can be expected to satisfy the minimum detection threshold in the low external noise limit, while also producing the maximum achievable SNR in the high external noise limit (i.e. be in the horizontal asymptotic region in Fig. 4A). The region where the black line deviates from the dashed line but has yet to converge with the light grey line corresponds to the mixed case in Fig. 4A and shows the range of  $n_{ext}/m^2$  where the  $A_{eff} = 500$  m<sup>2</sup> case fails to meet the desired

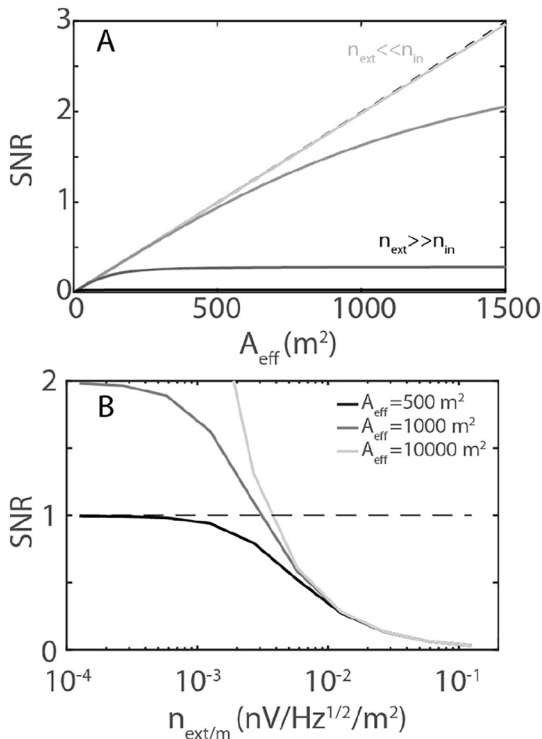


**Fig. 4.** A) SNR as a function of  $A_{\text{eff}}$  for four different external noise levels (light grey to black solid lines for increasing external noise levels). The dashed black line corresponds to the case where no external noise (only input noise) is present. The black curve in A) is close to the x-axis. B) SNR as a function of external noise level for three different  $A_{\text{eff}}$ . The dashed line corresponds to SNR = 1. The SNR in both cases is calculated given  $S_{\text{NMR}/m^2} = 0.0125 \text{ nV/m}^2$ ,  $n_{\text{in}} = 1.78 \text{ nV/Hz}^{1/2}$ ,  $N_{\text{stack}} = 16$  and  $\text{BW} = 200 \text{ Hz}$ .

SNR target. In this intermediate range performance could still be improved by increasing the coil area; for example, the 1000 m<sup>2</sup> line produces SNR > 1 in the low  $n_{\text{ext}/m^2}$  limit while also closely approximating the asymptotic SNR value (light grey line) closely after crossing the dashed line. This indicates that the 1000 m<sup>2</sup> can either satisfy the minimum SNR = 1 condition or approximate the asymptotic SNR value over a wide range of  $n_{\text{ext}/m^2}$  values. If  $A_{\text{eff}}$  is increased further the intermediate range where SNR is < 1 but has not yet satisfied the asymptotic value will be even further reduced. Note that the noise levels in Fig. 4A and B are based upon a 16 stack measurement; if more or less stacks are collected the threshold should be scaled by the ratio of  $\sqrt{N_{\text{stack}}/16}$ .

In many cases the  $A_{\text{eff}} = 500 \text{ m}^2$  threshold may be too conservative (e.g. for large currents or higher water contents) but it represents a compromise where we aim to provide guidelines for designing receivers that can perform well under a wide range of conditions. Note that it is advisable to employ coils with much larger  $A_{\text{eff}}$  than this threshold if it is possible to achieve larger  $A_{\text{eff}}$  without increasing the dimensions of the coil dramatically. This could be achieved by adding additional windings to a multi-turn receive coil.

### 3.2. Complementary small receivers

The primary advantage of small receivers is more rapid deployment in the field, potentially allowing many more receive coils to be exploited in a single measurement. Jiang et al. (2015) demonstrated the great potential of such an approach in the context of a 2D surface NMR measurement. We now consider a similar survey design, with the exception that multiple receive coils are to be used for the standard 1D depth profile experiment. We consider two scenarios, the first employs a 100 m by 100 m square transmit coil and several small receive coils embedded within the transmit coil. The second scenario considers the case where the large transmit loop is also used to receive the NMR signal in addition

to several small receive coils. The first scenario is used to test the hypothesis that the differing sensitivity profiles of receivers located at different locations in the transmit coil (which Fig. 3 clearly demonstrates can lead to varying signal amplitudes) can be used to enhance the resolution of surface NMR water content and relaxation time depth (1D) profiles. The second scenario investigates a practical survey design, where the large transmit loop is employed as a receiver in addition to several small receivers. Given that much effort goes into the careful deployment of the transmit loop, not employing it as a receiver represents a missed opportunity.

To evaluate whether the use of multiple small receive coils at varying locations can be used to improve spatial resolution we use the singular value decomposition (SVD) approach discussed by Müller-Petke and Yaramanci (2008). The SVD approach allows the resolution to be estimated from the SVD of the kernel matrix  $\mathbf{K}$ . To include noise considerations into the resolution calculations the singular values of the kernel matrix  $\mathbf{K}$  must be considered, as they affect how many basis vectors can be used during the calculation of the resolution matrix  $\mathbf{R}$  (Müller-Petke and Yaramanci, 2008). The advantage of the resolution matrix is that it is not dependent on a particular subsurface model (beyond influencing how many singular values are included) allowing it to provide general insight into the expected resolution offered by a particular survey design. To determine the resolution as a function of depth we use the full-width at half maximum of each row in the resolution matrix to determine a representative value for the resolution. To investigate the potential of multiple receivers to improve resolution we examine the SVD of a kernel matrix formed by concatenating the individual kernel matrices for each receiver. That is,  $\mathbf{K}_{\text{tot}}$  (the kernel matrix for the combined receiver case) is equal to  $[\mathbf{K}_1; \mathbf{K}_2; \dots; \mathbf{K}_n]$ , where  $\mathbf{K}_i$  is the kernel corresponding to the  $i$ th receiver. Fig. 5E illustrates the location of three 1 m by 1 m receivers located at different positions within the transmit loop; the receivers are centered at [0 0], [30,0], and [-30,0] (where [x y] represents the center of the coil in meters) and have effective areas of 500 m<sup>2</sup>. Fig. 5A and C illustrate the singular values associated with the individual kernels, and kernels formed by combining several of the receivers. The top and middle rows correspond to the same 40 ms on-resonance and adiabatic pulse used to form Fig. 2. The singular values associated with the individual kernels (blue, red, and green) decay at similar rates, with the kernels located at [-30 0] and [30 0] decaying slower than the kernel corresponding to the [0 0] receiver. For the combined kernel cases (where magenta corresponds to the combination of the [0 0] and [30 0] receivers, and black corresponds to the combination of all three receivers) the singular values are observed to improve in amplitude and decay at a slower rate. This suggests that given a particular noise level the calculation of the resolution matrix may include several additional singular values for the combined receiver kernels compared to the individual kernels. Fig. 5B and D illustrate the expected resolution as a function of depth for the same conditions investigated in 5A and 5C (i.e. colors correspond to the same scenario). The resolution matrix was calculated using only singular values that exceed a certain threshold, determined using a Picard plot given an external noise level equivalent to 50 nV of noise in a 10,000 m<sup>2</sup> coil, an internal noise level of 6.3 nV ( $n_{\text{in}} = 1.78 \text{ nV/Hz}^{1/2}$ ,  $N_{\text{stack}} = 16$  and  $\text{BW} = 200 \text{ Hz}$ ) and signal amplitudes that would be produced by a 30% water content half-space. The chosen noise levels and half-space conditions represent a simple scenario to gain insight into potential resolution benefits; actual resolution benefits will be dependent on local noise and signal amplitudes. Fig. 5B and D indicate that the resolution provided by the combined kernel cases (magenta and black) is improved over the full depth range compared to each of the individual cases. The resolution for the individual cases approach that provided by the combined kernels over limited depth ranges (e.g. the [-30 0] and [30 0] provide similar resolution at shallow depths, while the [0 0] case provides similar resolution at greater depths) but the combined scenarios provide the best resolution over the full depth range. The source of the improved resolution is the increased number of singular values included during the

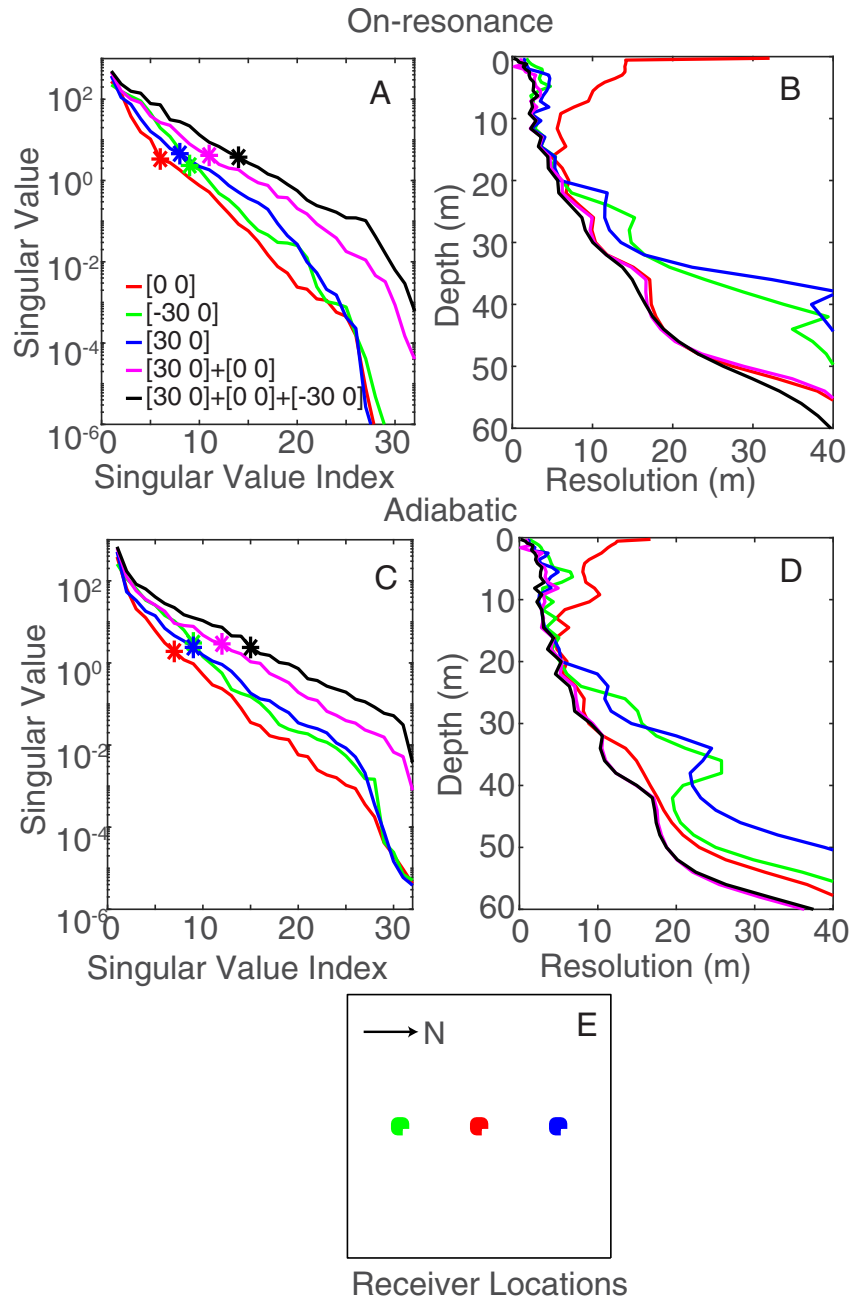


**Fig. 5.** Comparison of the singular values (A and C) and expected resolution (B and D) for several survey designs consisting of a small receiver and a 100 by 100 m transmitter. The top and middle rows correspond to the same on-resonance and adiabatic pulse investigated in Fig. 2, respectively. E) illustrates the location of each receiver. Note that the magenta and black lines in A–D) correspond to combinations of the receiver locations in E). Colors correspond to the relevant survey configuration (blue, red, and green correspond to single receiver scenarios, while magenta and black correspond to scenarios that employ multiple receivers). Stars in A) and C) indicate the smallest singular value used to calculate the resolution in B) and D). Note that the magenta line in D) is mostly overlain by the black line.

calculation of the resolution matrix (the stars in Fig. 5A and C indicate the smallest singular value that exceeds the threshold set by the noise floor in this example, where the magenta and black stars are observed to occur for larger singular value indices than for the individual cases).

Consider next a more practical scenario, where the large transmit coil is also employed as a receiver. Fig. 6A and C illustrate the singular values for several combined receiver scenarios, as well as the singular values associated with the 100 m receive loop only case (red). The top and bottom rows again correspond to the same 40 ms on-resonance and adiabatic pulses considered in Fig. 2. The green, blue, and black lines correspond to the cases where the 100 m receive loop is used in combination with the [30 0] receiver, the [30 0] and [0 0] receivers,

and all three small receivers, respectively. This represents surveys employing 2, 3, and 4 receivers. In this case, the addition of the small receivers slows the decay of the singular values. The largest singular values are not significantly affected, but the decay for singular values corresponding to indices larger than ~18 is significantly reduced. The addition of more receivers slows the decay even further. This again suggests that the use of complementary small receivers may admit the inclusion of additional singular values during the calculation of the resolution matrix. Fig. 6B and D illustrate the expected resolution as a function of depth for the same scenarios considered in Fig. 6A and C. The same noise and half-space conditions as in Fig. 5 are used to determine the threshold below which the singular values are truncated. The combined cases are observed to improve resolution compared to the

single large receiver case (red). The resolution improvement is observed to be stronger for the on-resonance pulse compared to the particular adiabatic pulse investigated. In each case, the inclusion of additional receivers continues to improve resolution (e.g. the 4 receiver case provides better resolution compared to the 3 receiver case over the full depth range). The source of the improved resolution is again the inclusion of additional singular values, observed by noting the location of the smallest singular value exceeding the threshold (denoted by stars in Fig. 6A and C). In summary, Fig. 6 indicates that even in the 1D (depth profile) scenario, the use of complementary small receive coils (in addition to a large receiver) can help to improve the resolution of the estimated water content and relaxation time depth profiles. If the complementary receiver coils are small, their associated benefits can be exploited without significant increases in survey times.

### 3.3. Field measurements with small receive coils

To demonstrate the feasibility of a small surface NMR receiver (with effective areas similar to the proposed threshold of  $\sim 500 \text{ m}^2$ ) field measurements were conducted near Skanderborg, Denmark using two small receive coils in conjunction with a 100 m by 100 m square transmitter and a 40 ms on-resonance pulse. The goal is to demonstrate that subsurface model produced by each of the two small receivers are consistent with each other and with a priori information about the site

based on TEM measurements that indicate a thick resistive unit (interpreted to be a thick sand layer) extending to depths of  $\sim 30 \text{ m}$  underlain by a more conductive unit (interpreted to be a finer sand/clayey sand layer). The NUMIS-poly system was employed as a transmitter with 16 pulse moments ranging from 0.74 As to 8.3 As and 20 stacks. The Apsu receive system was used to record the surface NMR signal. The surface NMR signal was recorded by two receive coils, the first was a 2.5 m by 2.5 m square with 32 turns and the second was a 5 m by 5 m square with 16 turns that correspond to effective areas of  $200 \text{ m}^2$  and  $400 \text{ m}^2$ , respectively. These coil areas were chosen as they represented the most convenient approximations to the recommended  $500 \text{ m}^2$  target given the employed receive coils which are composed of cables of length 40 m with 4 twisted pairs. Both receivers were centered at [30 0] m. Fig. 7C and E illustrate the measured data cubes; each data cube is observed to be very similar (as expected) with the signal amplitudes scaled by the respective differences in effective area (i.e. the  $400 \text{ m}^2$  coil's signal is twice as large as that measured by the  $200 \text{ m}^2$  coil, noted by the factor of two difference in the color bars). Fig. 7A and B illustrate the water content and  $T_2^*$  profiles estimated in each case. The inversion was performed using AarhusInv (Auken et al., 2014), and amplitude-only data (the signal phase was not included). Data were gated into fourteen logarithmically spaced gates, with the first gate centered at 25 ms and the final gate at 323 ms; the  $200 \text{ m}^2$  and  $400 \text{ m}^2$  coil data were treated with standard deviations of 5 nV and 10 nV,

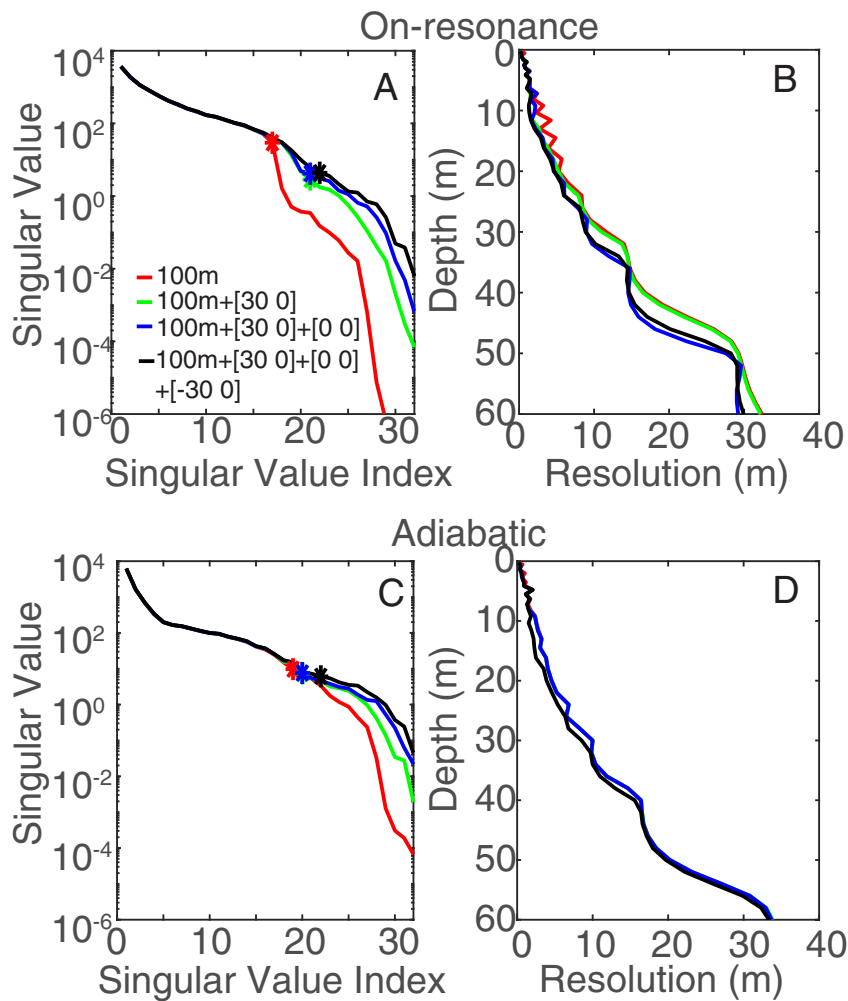


**Fig. 6.** Comparison of the singular values (A and C) and expected resolution (B and D) for several survey designs employing a 100 m coincident Tx/Rx coil in addition to complementary small receiver coils. The top and bottom rows correspond to the same on-resonance and adiabatic pulse investigated in Fig. 2, respectively. The small receivers are located at the same positions as in Fig. 5. Colors correspond to the relevant survey configuration (red is the 100 m Rx only, while green, blue, and black correspond to scenarios where small receive coils are used in addition to the 100 m Rx coil). Stars in A) and C) indicate the smallest singular value used to calculate the resolution in B) and D). The red and green lines in D are mostly overlain by the blue line.

respectively, during the inversion. The conductivity structure at the site was estimated by a ground-based TEM measurement and was fixed during the inversion. Both sets of profiles produce similar results, predicting the presence of a thick water bearing unit beginning at ~7 m depth with a peak water content of ~30% at 10–15 m depth. At greater depths the water content trends to a lower values (over the depth range from 15 to 30 m) and estimates a relatively constant value of ~10% below 30 m. The corresponding data misfits are illustrated in Fig. 7D and F (the illustrated misfits are equal to modelled data minus the observed data). Fig. 7G and H illustrate histograms of the misfits in Fig. 7E and F and demonstrate that the data is fit within error (i.e. the misfits in each case are similar magnitudes to the standard deviations used to weight the data in the inversion). The histograms indicate that

the misfit for the 200 and 400 m<sup>2</sup> coils is quite similar, but where the 400 m<sup>2</sup> histogram appears to be slightly wider than the 200 m<sup>2</sup> case. Note that the histograms display widths slightly larger than that expected from the internal noise levels, where an RMS internal noise level of ~5.6 nV is expected given  $n_{in} = 1.78 \text{ nV/Hz}^{1/2}$ ,  $N_{stack} = 20$  and  $BW = 200 \text{ Hz}$ . Overall, Fig. 7 demonstrates the feasibility of a small surface NMR receiver. Although Fig. 7 also demonstrates that receivers smaller than the recommended  $A_{eff} 500 \text{ m}^2$  are possible, it is still recommended to use larger  $A_{eff}$  if possible.

The similar widths of the misfit histograms in Fig. 7 suggest that the noise in both data sets illustrated in Fig. 7 is strongly influenced by internal noise sources. The internal noise levels in both cases is the same (as its controlled by electronics), while external noise should scale with the

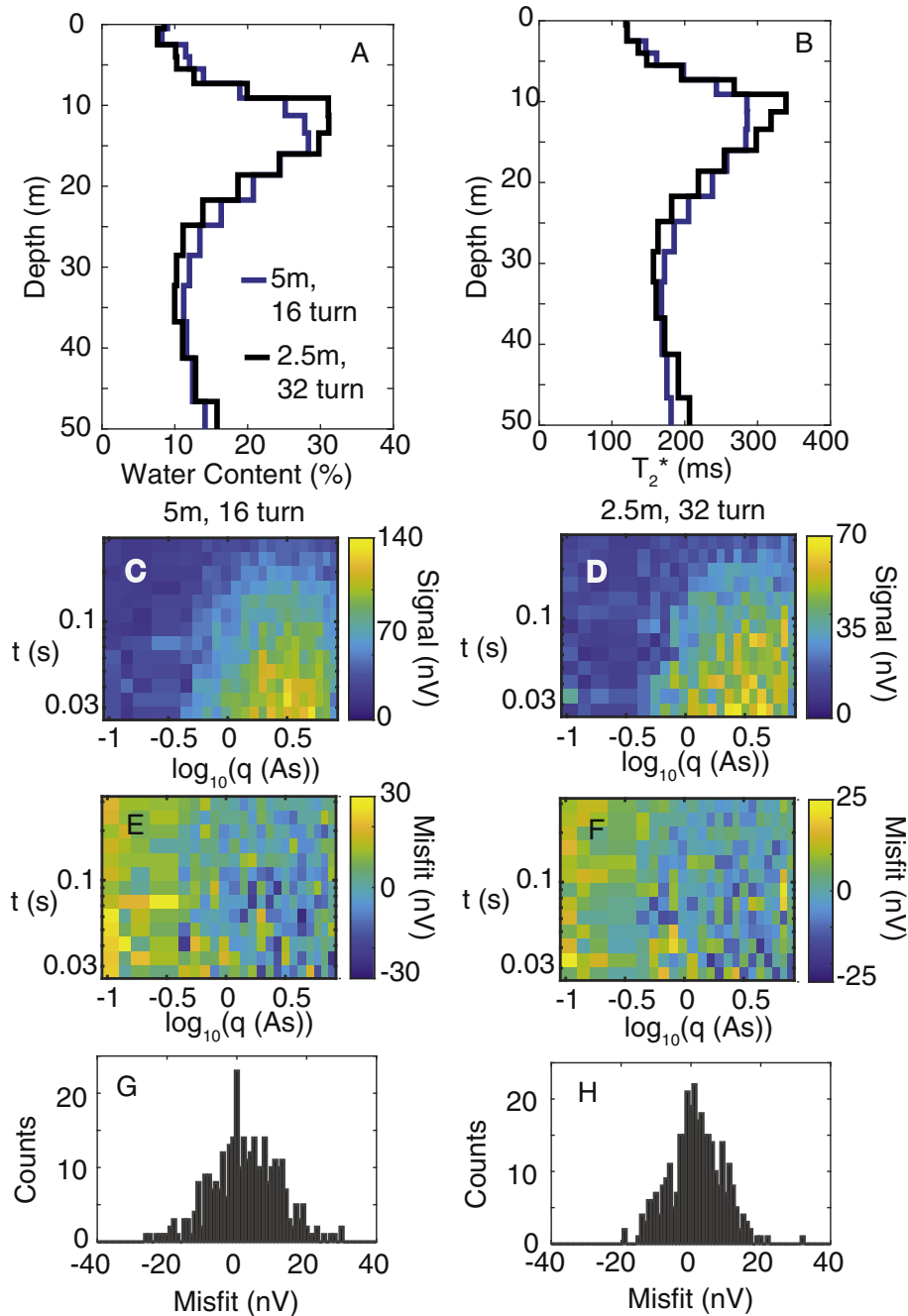


**Fig. 7.** A) and B) illustrate the estimated water content and  $T_2^*$  profiles produced using a 2.5 m by 2.5 m 32 turn receive coil and a 5 m by 5 m 16 turn receive coil and a square 100 m transmit loop. C), E), and G) illustrate the processed data, data misfit for the final model (modelled data – observed data), and a histogram of the misfits for the 5 m receive coil, respectively. D), F), and H) illustrate the processed data, data misfit for the final model (modelled data – observed data), and a histogram of the misfits for the 2.5 m receive coil, respectively.

coil area. If external noise was dominant we would expect the 400 m<sup>2</sup> histogram to be twice as wide as the 200 m<sup>2</sup> histogram. Furthermore, if external noise was the dominant noise mechanism we could expect that during a noise-only time series the voltages in each coil should track one another closely and simply be scaled by the ratio of effective areas since the two coils are centered at the same location and measure synchronized data. Fig. 8 shows a histogram of the coherence squared magnitude between the two receive coils for a set of 300 ms long time windows beginning 600 ms after the end of each pulse (raw data). In total, the histogram is formed from 460 separate 300 ms long windows. The magnitude squared coherence is binned into 100 bins each 0.01 wide. Frequencies with poor and strong coherence correspond to histograms with black bins close to 0 and 1, respectively. For most of the frequency band of interest the coherence is much less than 1. Only at a few frequencies that correspond to power line harmonics (e.g. 1.1 and 1.3 kHz) is strong coherence observed. The overall lack of coherence suggests that the primary noise source present in each receiver is internal noise; if the dominant noise source was external noise we would obtain a much stronger coherence between the two receivers. This suggests that a further reduction in effective area will degrade the net SNR even further given that the internal noise levels do not scale with coil area.

#### 4. Discussion

A desire to use small receivers is motivated by the need to reduce the surface NMR measurement time and improve resolution. Based on the input noise of the receivers employed in this study (1.78 nV/Hz<sup>1/2</sup>) and a minimum stack number of 16 stacks a lower  $A_{eff}$  threshold of ~500 m<sup>2</sup> is recommended for signal detection receive loops. Receive coils intended to measure only noise (reference coils) may be smaller at ~200 m<sup>2</sup>. Note that if possible it is advisable to exceed these thresholds in order to further reduce concerns related to  $n_{int}$  and to expand the range of external noise conditions where the receiver will still satisfy the SNR = 1 threshold (e.g. Fig. 4B). Given that receivers below ~15 m in side length perform very similarly (i.e. produce similar sounding curves in Fig. 2) two parameters can be manipulated to produce a desired  $A_{eff}$ . The first is the coil side length and the second is the number of turns. Increasing the coil side length provides an easy approach to increase  $A_{eff}$ , but this strategy is somewhat counter to the stated goals of working with small receivers. Ideally, the receiver's physical dimensions can be reduced as much as possible. However, one limitation to working with very small coils with large numbers of turns is that the self-capacitance and inductance of the receive coil may increase causing the coil's cutoff frequency to approach the frequency band of interest (1–3 kHz). In practice the lower limit on coil size will be set by the

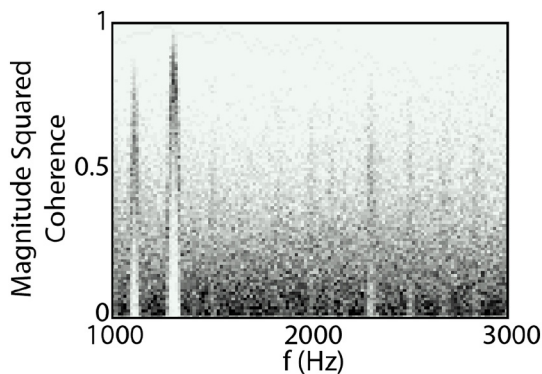


Fig. 8. Histograms showing the coherence between the data measured (during a noise only window from 600 to 900 ms following the excitation pulse) in the 2.5 m and 5 m receivers that are located at the same center point for 460 different time intervals. Black pixels correspond to bins containing 25 counts, while white pixels correspond to bins containing 0 counts.

ability to attain the minimum effective area without dropping the coil's cutoff frequency to values near the Larmor frequency (e.g. cutoff frequencies should be greater than ~5–10 kHz). If the coil's cutoff frequency approaches a few kHz the coil gain may no longer be equal to 1 in the frequency band of interest, which may result in an increased contribution of Johnson noise. In this limit the criteria used to determine the recommended thresholds should be adjusted to include Johnson noise. To include Johnson noise Eq. (1) can be added in series with the other noise terms under the square root in Eq. (5). Note that if Johnson noise is to be included this requires the coil shape/size to be specified as  $n_j$  scales with the length of the wire while the signal and external noise scale with the coil area. A tuned receiver also has the disadvantage that induced currents due to the transmit pulse will decay more slowly resulting in an increased dead time. It is also important to ensure that the coil is damped correctly, otherwise the coil gain in the frequency band of interest may not be equal to 1. The resonance frequency of the small coils should be measured to ensure their resonance frequencies are much greater than the Larmor frequency (the receive coils used in the field study have resonance frequencies above ~40 kHz). Overall, this work provides insight into the necessary constraints for the design of small surface NMR receivers, which could present significant reductions in measurement times for multi-receive coil surface NMR experiments. Construction of small rigid surface NMR receivers is the focus of future work.

In the pursuit of small surface NMR receive coils the limiting noise factor in the untuned receiver scenario is likely to be the preamplifier input noise. This is due to the fact that as the coil's effective area decreases so does the measured signal, ultimately approaching the noise level set by the preamplifier. The decision to recommend a minimum  $A_{eff}$  area based upon a noise threshold set by the internal noise attempts to provide a general recommendation based on predictable values such as  $S_{NMR/m^2}$  for a low water content half-space and known input noise levels. Note that the recommendation of  $A_{eff} = 500$  m<sup>2</sup> does not satisfy the SNR = 1 target for all  $n_{ext/m^2}$ ; at low  $n_{ext/m^2}$   $A_{eff} = 500$  m<sup>2</sup> approaches SNR = 1 and at high  $n_{ext/m^2}$  it approximates the SNR expected for a much larger coil. To expand the range of  $n_{ext/m^2}$  where the coil satisfies the SNR = 1 target a larger  $A_{eff}$  can be selected. As long as the coil's  $A_{eff}$  is capable of satisfying the condition that  $S_{net} \gg n_{in}$ , increasing  $A_{eff}$  by adding additional turns will not improve SNR in practice.  $S_{NMR/m^2}$  and  $n_{ext/m^2}$  are both proportional to  $A_{eff}$  and thus effectively lock the single stack SNR. If  $n_{ext/m^2}$  is much larger than  $S_{NMR/m^2}$  there unfortunately is not much that can be done, the noise conditions are poor and scaling  $A_{eff}$  cannot address the low SNR problem.

To further reduce  $A_{eff}$  below the recommended threshold several options are possible. Alternative preamplifier design may help to reduce the  $n_{in} = 1.78$  nV/Hz<sup>1/2</sup>, which would ultimately lower the noise thresholds used to select  $A_{eff}$ . For example, an unbalanced coil that uses a single preamplifier may help lower the recommended  $A_{eff}$  threshold at the expense of increased common mode noise. Secondly, the threshold aims to ensure adequate signal amplitudes even at low pulsed current amplitudes that produce the smallest signals in Figs. 2 and 3. If only larger currents (e.g. currents greater than ~5–10 A) are used the threshold may be further reduced. However, choosing to not collect low pulsed current data may reduce resolution at shallow depths. Note that selecting a favorable receiver location (e.g. north half of the transmit loop) and excitation scheme (e.g. adiabatic pulses that produce larger signal amplitudes) may also help to reduce this threshold. The recommended threshold aims to provide adequate signal amplitudes even in low signal amplitude scenarios (e.g. low water content, small currents). If possible, it is recommended that receivers with much larger  $A_{eff}$  than the proposed threshold of 500 m<sup>2</sup> be employed. Note that if an alternative system with a different input noise level is used, the minimum  $A_{eff}$  calculation should be adjusted to reflect that system's input noise.

Another advantage of small NMR receivers is that they can effectively be modelled as dipoles; that is, the  $B_1$  field originating from the

small receive coils is well-described by a dipole whose moment is scaled to produce an equivalent  $A_{\text{eff}}$ . It is also important to ensure that the grid used in the forward modelling is refined around the location of the receive coil in order to limit numerical inaccuracies. For the AarhusInV surface NMR forward modelling, the grid is Cartesian and is locally refined in the close vicinity of all wires. The transmit and receive  $B_1$  fields also share a grid. For alternative modelling approaches, such as schemes that employ a cylindrical coordinate system, it is important to locally refine the grid around the receive coils. Note that accurately describing the receiver location within the transmit loop is also extremely important.

The use of multiple small receive coils is naturally suited to 2D/3D surface NMR surveys (Jiang et al., 2015). However, even in surveys intended to produce only 1D depth profiles, the use of multiple small receive coils is still beneficial due to potential resolution benefits. It is recommended that the large transmit coil also functions as a receiver, and that smaller receive coils can be used as complements to help improve resolution. Given that much effort goes into careful deployment of the transmit coil, neglecting its use as a receive coil would be a wasted opportunity since it is also exhibits a differing spatial sensitivity compared to smaller receive coils (noted by comparing the 100 m receiver with the 1 m receiver in Fig. 2). Exploitation of additional small, easily deployed receive coils offers great potential to improve the resolution of surface NMR water content and  $T_2^*$  depth profiles.

Several other studies have also investigated the feasibility of small receive coils for underground MRS applications. For example, Greben et al. employed a 3 m by 3 m 128 turn coil but high noise conditions in the mine made it difficult reliably detect an NMR signal. Lin et al. (2017) demonstrated the feasibility of a small nitrogen-cooled 1 m by 1 m 80 turn receive coil that was used in conjunction with a single turn 1 m by 1 m transmit coil. The receiver design considered by Lin et al. (2017) differs from this study in that they employ a tuned receive coil, which leads to increased concerns about Johnson noise. The conditions considered in this study also differ from those in underground MRS in that we consider the case where a large (100 m by 100 m) transmitter is used in conjunction with a small receiver, whereas underground MRS must also work with geometry constraints for the transmit coil.

## 5. Conclusions

The use of multiple receive coils in surface NMR presents several benefits, such as rapid collection of 2D/3D surface NMR data and improved noise cancellation through the use of a reference loop. To help facilitate more rapid field deployment and fully exploit these approaches small receive coils are desirable. An investigation into several practical limitations on the minimum size of surface NMR receivers is presented. The threshold for a minimum receiver size is proposed based upon limits imposed by the receiver's input noise level (which based on the surface NMR instrumentation used in this study is  $\sim 1.78$  nV/Hz<sup>1/2</sup>) and a signal amplitude expected from a 5% water content half-space. Given this scenario, the minimum recommended effective area for a surface NMR receiver is approximately 500 m<sup>2</sup>. Smaller receive coils may be exploited provided advances in preamplifier design, larger minimum stack numbers, and by selecting favorable receiver location/excitation protocols (e.g. particular current amplitudes and pulse types). To expand the range of noise conditions where the coil can be expected to satisfy the minimum SNR = 1 criteria the coil area can be increased to values larger than 500 m<sup>2</sup>. The use of several small receive coils is also demonstrated to improve depth resolution for a 1D surface NMR survey. Placement of small receive coils in the northern half of the transmit coil is recommended (for the northern hemisphere, the southern half is recommended for the southern hemisphere) in order to exploit an asymmetry present in the spatial distribution of the excited magnetization due to the inclination of the Earth's magnetic field. Note that if possible (i.e. without scaling the dimensions of the

receive coil dramatically) coils with effective areas exceeding the recommended threshold should be employed. Ultimately, small receive coils present an opportunity to enhance the utility of surface NMR measurements.

## Acknowledgements

Denys Grombacher was supported by funding from a Danish Council for Independent Research Postdoctoral Grant (DFF-5051-00002). This work was also supported by grants from the Aarhus University Research Foundation and the COWI Foundation.

## References

- Auken, E., Christiansen, A.V., Kirkegaard, C., Fiandaca, G., Schamper, C., Behroozmand, A.A., Binley, A., Nielsen, E., Efferso, F., Christensen, N.B., Sorensen, K.I., Foged, N., Vignoli, G., 2014. An overview of a highly versatile forward and stable inverse algorithm for airborne, ground-based and borehole electromagnetic and electric data. *Explor. Geophys.* 46 (3), 223–235.
- Behroozmand, A.A., Auken, E., Fiandaca, G., Christiansen, A.V., Christensen, N.B., 2012. Efficient full decay inversion of MRS data with a stretched-exponential approximation of the  $T_2^*$  distribution. *Geophys. J. Int.* 190 (2), 900–912.
- Behroozmand, A.A., Auken, E., Fiandaca, G., Rejkaer, S., 2016. Increasing the resolution and the signal-to-noise ratio of magnetic resonance sounding data using a central loop configuration. *Geophys. J. Int.* 205 (1), 243–256.
- Carlson, J.W., Minemura, T., 1993. Imaging time reduction through multiple receiver coil data acquisition and image reconstruction. *Magn. Reson. Med.* 29 (5), 681–687.
- Costabel, S., Müller-Petke, M., 2014. Despiking of magnetic resonance signals in time and wavelet domains. *Near Surf. Geophys.* 12, 185–197.
- Dalgaard, E., Auken, E., Larsen, J.J., 2012. Adaptive noise cancelling of multichannel magnetic resonance sounding signals. *Geophys. J. Int.* 191, 88–100.
- Dalgaard, E., Christiansen, P., Larsen, J.J., Auken, E., 2014. A temporal and spatial analysis of anthropogenic noise sources affecting SNMR. *J. Appl. Geophys.* 110, 34–42.
- Davis, A.C., Dlugosch, R., Queitsch, M., Macnae, J.C., Stolz, R., Müller-Petke, M., 2014. First evidence of detecting surface nuclear magnetic resonance signals using a compact B-field sensor. *Geophys. Res. Lett.* 41 (12), 4222–4229.
- Greben, J.M., Meyer, R., Kimmie, Z., 2011. The underground application of magnetic resonance sounding. *J. Appl. Geophys.* 75 (2), 220–226.
- Grombacher, D., 2018. Numerically optimized modulations for adiabatic pulses in surface NMR. *Geophysics* 83 (2), JM1–JM14.
- Grunewald, E., Walsh, D., 2016. Development of rapid scanning surface-NMR for wide area hydrogeologic mapping. ASEG Extended Abstracts, Adelaide, Australia, August 21–24.
- Hertrich, M., Braun, M., Yaramanci, U., 2005. Magnetic resonance soundings with separated transmitter and receiver loops. *Near Surf. Geophys.* 3 (3), 141–154.
- Hertrich, M., Braun, M., Gunther, T., Green, A.G., Yaramanci, U., 2007. Surface nuclear magnetic resonance tomography. *IEEE Trans. Geosci. Remote Sens.* 45 (11), 3752–3759.
- Hertrich, M., Green, A.G., Braun, M., Yaramanci, U., 2009. High-resolution surface NMR tomography of shallow aquifers based on multioffset measurements. *Geophysics* 74 (6), G47–G59.
- Jiang, C., Lin, J., Duan, Q., Sun, S., Tian, B., 2011. Statistical stacking and adaptive notch filter to remove high-level electromagnetic noise from RMS measurements. *Near Surf. Geophys.* 9, 459–468.
- Jiang, C., Müller-Petke, M., Lin, J., Yaramanci, U., 2015. Magnetic resonance tomography using elongated transmitter and in-loop receiver arrays for time-efficient 2-D imaging of subsurface aquifer structures. *Geophys. J. Int.* 200 (2), 824–836.
- Kass, M.A., Irons, T.P., Behroozmand, A., Grombacher, D., Bloss, B.R., 2017. Surface nuclear magnetic resonance with compact multicomponent receivers. *Near Surface 2017 – 23th European Meeting of Environmental and Engineering Geophysics*, Malmö, Sweden, September 3–7.
- Larsen, J.J., 2016. Model-based subtraction of spikes from surface nuclear magnetic resonance. *Geophysics* 81 (4), WB1–WB8.
- Larsen, J.J., Dalgaard, E., Auken, E., 2014. Noise cancelling of MRS signals combining model-based removal of powerline harmonics and multichannel Wiener filtering. *Geophys. J. Int.* 196, 828–836.
- Legchenko, A., 2007. MRS measurements and inversion in presence of EM noise. *Bol. Geol. Min.* 118, 489–508.
- Legchenko, A., Valla, P., 2002. A review of the basic principles for proton magnetic resonance sounding measurements. *J. Appl. Geophys.* 50 (1–2), 3–19.
- Legchenko, A., Valla, P., 2003. Removal of power-line harmonics from proton magnetic resonance measurements. *J. Appl. Geophys.* 53 (2–3), 103–120.
- Legchenko, A., Desclotres, M., Vincent, C., Guyard, H., Garambois, S., Chalikhakis, K., Ezersky, M., 2011. Three-dimensional magnetic resonance imaging for groundwater. *New J. Phys.* 13, 025022.
- Lin, J., Du, G., Zhang, J., Yi, X., Jiang, C., Lin, T., 2017. Development of a rigid one-meter-side coil and cooled coil sensor at 77 K for magnetic resonance sounding to detect subsurface water sources. *Sensors* 17, 1362.
- Liu, L., Grombacher, D., Larsen, J., Auken, E., 2017. A multi-channel, low noise surface NMR receiver system with wireless connections to signal and reference coils. *Near Surface 2017 – 23th European Meeting of Environmental and Engineering Geophysics*, Malmö, Sweden, September 3–7.

- Müller-Petke, M., Costabel, S., 2014. Comparison and optimal parameter settings of reference based harmonic noise cancellation in time and frequency domains for surface-NMR. *Near Surf. Geophys.* 12 (2), 199–210.
- Müller-Petke, M., Yaramanci, U., 2008. Resolution studies for magnetic resonance sounding (MRS) using the singular value decomposition. *J. Appl. Geophys.* 66 (3–4), 165–175.
- Nyboe, N.S., Sørensen, K., 2012. Noise reduction in TEM: presenting bandwidth- and sensitivity-optimized parallel recording setup and methods for adaptive synchronous detection. *Geophysics* 77 (3), E203–E212.
- Plata, J., Rubio, F., 2002. MRS experiments in a noisy area of a detrital aquifer in the south of Spain. *J. Appl. Geophys.* 50, 83–94.
- Pruessmann, K.P., Weiger, M., Scheidegger, M.B., Boesiger, P., 1999. SENSE: sensitivity encoding for fast MRI. *Magn. Reson. Med.* 42, 952–962.
- Pruessmann, K.P., Weiger, M., Boesiger, P., 2001. Sensitivity encoded cardiac MRI. *J. Cardiovasc. Magn. Reson.* 3 (1), 1–9.
- Radic, T., 2006. Improving the signal-to-noise ratio of surface NMR data due to the remote reference technique. *Near Surface 2006 – 12th European Meeting of Environmental and Engineering Geophysics*, Helsinki, Finland, September 4–6.
- Trushkin, D.V., Shushakov, O.A., Legchenko, A.V., 1994. The potential of a noise-reducing antenna for surface NMR groundwater surveys in the earth's magnetic field. *Geophys. Prospect.* 42 (8), 855–862.
- Walsh, D.O., 2008. Multi-channel surface NMR instrumentation and software for 1D/2D groundwater investigations. *J. Appl. Geophys.* 66 (3–4), 140–150.
- Weichman, P.B., Lavelly, E.M., Ritzwoller, M.H., 2000. Theory of surface nuclear magnetic resonance with applications to geophysical imaging problems. *Phys. Rev. E* 62, 1290–1312.
- Weiger, M., Pruessmann, K.P., Boesiger, P., 2002. 2D SENSE for faster 3D MRI: magnetic resonance in materials in physics, biology, and medicine. *14* (1), 10–19.